Impact pressures and flow regimes in dense snow avalanches observed at the Vallée de la Sionne test site

Betty Sovilla,[1] M. Schaer,[1] M. Kern,[1] and P. Bartelt[1]

[1] A fundamental problem in avalanche engineering is to determine the impact pressures exerted on structures. This task is complicated because snow avalanches flow in a variety of regimes, primarily depending on snow temperature and moisture content. In this paper we address this problem by analyzing measured impact pressures, flow velocities, and flow depths of five Vallée de la Sionne avalanches. The measurements are made on a 20 m high tubular pylon instrumented with high-frequency pressure transducers and optoelectronic velocity sensors. In the observed avalanches, we find both subcritical and supercritical flow regimes. Typical Froude numbers were smaller than 6. The subcritical regime ($Fr < 1$) is characterized by a flow plug riding above a highly sheared basal layer. The measured pressures are large and velocity-independent in contradiction to calculation procedures. Pressure fluctuations increase with flow depth, indicating a kinematic stick-slip phenomena which is largest at the basal layer. Supercritical flow regimes ($1 < Fr < 6$) are characterized by a sheared flow all over the avalanche depth. In this regime the impact pressure is velocity-dependent. We derive relationships governing impact pressure as a function of the Froude number, and therefore flow regime, encompassing all the observed avalanches.

Citation: Sovilla, B., M. Schaer, M. Kern, and P. Bartelt (2008), Impact pressures and flow regimes in dense snow avalanches observed at the Vallée de la Sionne test site, *J. Geophys. Res.*, *113*, F01010, doi:10.1029/2006JF000688.

1. Introduction

[2] A common task in snow engineering is to design structures that must withstand the dynamic loadings of dense, flowing avalanches. The first step in solving such problems is to estimate the maximum possible avalanche flow velocities as a function of the avalanche return period. Although velocities can be estimated in three-dimensional terrain with the help of numerical models, there exists no accurate relationship to find the avalanche impact pressures, given the avalanche velocity and density. This is in large part due to the fact that existing hydrodynamic formulas for the impact pressure do not take into account the wide range of avalanche flow regimes, which can vary between wet, viscous flows to dry, granular flows [*Savage and Hutter*, 1991; *Norem et al.*, 1987, 1989]. In this paper we address this problem by studying measurements of avalanche impact pressures as a function of the avalanche flow regime. The measurements were performed at the Vallée de la Sionne (VdlS) avalanche test site between the years 2003 and 2005 (Figure 1).

[3] Early pressure measurements in VdlS (made during the catastrophic avalanche winter of 1999) indicated the existence of different flow structures, e.g., dense flow layers and saltation layers [*Schaer and Issler*, 2001]. These layers were distinguished by observation of pressure measurements. The dense layer is characterized by a continuously acting pressure, which indicates a continuous flow medium. The saltation layer is characterized by high, short peaks which are separated by pressure values dropping to zero. These peaks were interpreted as impacts of saltating clods of snow surrounding the dense core.

[4] Although in good agreement with previous observations from impact pressures in snow avalanches [*Schaerer and Salway*, 1980; *McClung and Schaerer*, 1985; *Norem et al.*, 1985], the measurements provided little additional information because the local velocities, densities and flow heights, the data needed to characterize the flow regime, remained unknown. Therefore, after the 20 m high pylon (Figure 2) was destroyed by a large avalanche in 1999 it was rebuilt in 2002 and instrumented with optoelectronic sensors [*Tiefenbacher and Kern*, 2004], capacitance-based density probes [*Louge et al.*, 1997], pitot sensors [*McElwaine and Turnbull*, 2005] and simple toggle switches that effectively capture the dense flow height and transition layer to the powder cloud [*Sovilla and Bartelt*, 2002]. The velocity sensors were spatially distributed on the mast to obtain the best possible resolution of the velocity gradients in the dense layer. These local, point measurements can be coupled with the photogrammetric [*Vallet et al.*, 2001] and video-grammetric measurements [*Vallet et al.*, 2004] that provide

---

[1]Swiss Federal Institute for Snow and Avalanche Research, Davos, Switzerland.

Figure 1. Overview of the Vallée de la Sionne test site. Avalanche 629 is reaching the obstacle zone (circle).

additional information regarding the avalanche event, such as the strike angle of the avalanche with the mast and approximate release and entrained snow masses [*Sovilla et al.*, 2006].

[5] In the following we study the recorded impact pressure profiles in combination with the measured velocity profiles for five VdlS avalanches. Although we can study the profiles as a function of time (that is, as the avalanche passes our measurement pylon), we restrict our analysis to a time window where the maximum impact pressures are recorded. We identify two primary flow regimes: a plug flow regime, that is associated with wet snow avalanches and a sheared flow regime, located at the front of dry flowing avalanches. We characterize the flow regime not only by the shear rates in the avalanche core, but also by the corresponding Froude numbers. We begin by reviewing the pressure, velocity and flow height instrumentation at the VdlS test site.

2. Instrumentation and Methods

[6] The measurements presented in this paper have been performed at the Vallée de la Sionne test site [*Ammann*, 1999]. The site, located in the Swiss Alps, is perfect for the release of both dense and dilute large avalanches. A detailed description of the topographical characteristics and infrastructures can be found in work by *Issler* [1999].

[7] From the numerous measurements performed at Vallée de la Sionne, in this paper we analyze only data recorded at the oval-shaped steel mast shown in Figure 2.

[8] The tower is 20 m high, 0.6 m wide and 1.5 m long, thus it is high enough to record the impact and stagnation pressures in the dense, saltation and most of the suspension layer of avalanches. High-frequency load cells allow to resolve impacts of single snow clods in the different layers [*Schaer and Issler*, 2001]. By complementary considerations of the records with optical sensors for the determination of speed profiles [*Tiefenbacher*, 2003], capacitance probes for density measurements [*Louge et al.*, 1997] and

flow depth sensors, a complete set of the most important avalanche properties can be obtained. On the top of the mast, an acceleration sensor measures the motion of the obstacle induced by the flow [*Issler*, 1999].

[9] For the aim of this study we use pressure, velocity and flow depth measurements. As lined out below, unfortunately,
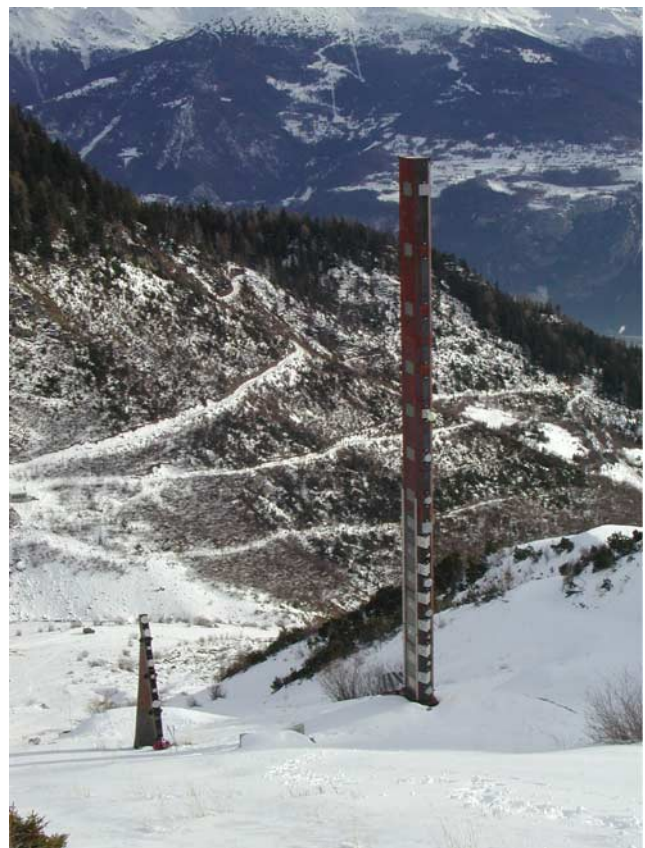

Figure 2. View of the 20 m high mast. It is instrumented with high-frequency load cells, optical sensors, and flow depth sensors.

Figure 3. View of sensors mounted on the mast. On the left are toggle switches; note that each sensor is protected by a small metal roof to avoid rupture by vertical load. In the middle are optical sensors flush mounted to a half wedge for better contact with the snow. On the right is a pressure sensor.

density measurements proved to have a too low definition to be useful.

2.1. Pressure Measurements

[10] Piezoelectric load cells are mounted with 1 m spacing along the mast from 0.5 to 5.5 m above the ground. During the winter season 2003–2004, sensor diameters were 0.1 and 0.25 m; since the winter season 2004–2005, all sensors have a diameter of 0.10 m. The sensors measure the pressure in the dense and saltation layers with a sampling frequency of 7.5 kHz. Details of the mast instrumentation are shown in Figure 3. The main technical characteristics of the sensors are described by *Schaer and Issler* [2001].

[11] In principle, the influence of varying sensor dimensions [*McClung and Schaerer*, 1985] can be analyzed with the described setup. A preliminary analysis of all pressure measurements performed at the Vallée de la Sionne test site found that average pressure appears to be independent of sensor dimension for sensor diameters between 0.1 m and 0.25 m [*Sovilla et al.*, 2008]. On the contrary pressure peak magnitude increases with decreasing sensor dimension.

2.2. Velocity Measurements

[12] The avalanche flow velocity is measured by opto-electronic sensors which are flush mounted to a wedge in front of the mast and the flow passing the sensors can be regarded as to be nearly undisturbed (Figure 3). The measurement principle is based on the cross correlation of the signals of two reflectivity sensors with a streamwise spacing [*Tiefenbacher and Kern*, 2004; *Dent et al.*, 1998]. The reflectivity signals of the sensors are captured with a sampling frequency of 20 kHz. See *Tiefenbacher and Kern* [2004] for a more detailed description.

[13] During the winter season 2003–2004, the optical sensors where installed at the tubular mast, at 1, 2, 3, 4, 5 and 6 m above ground and the flow velocities of four avalanches (No. 6236, 6237, 6241, and 629) have been recorded with this configuration (Table 1). During the summer 2004, the installation has been optimized by increasing the number of sensors in the lower part of the mast. Sensors are now installed at 1.25, 1.4, 1.55, 1.7, 2, 3, 4, and 5 m above ground. Avalanche 7226 has been measured with this configuration.

[14] Both configurations allow for an Eulerian description of the velocity field with a good spatial and temporal resolution.

[15] The error associated with the measurements increases with velocity: for dense avalanches the quality of the data (i.e., the definition of the maximum of the correlation integral) is reasonably high, whereas for more dilute avalanches the correlation of the signal becomes progressively difficult as the turbulent fields, with decreasing flow densities, lead to ambiguities when identifying the correlation integral maximum.

2.3. Flow Depth Measurements

[16] The flow depth of the dense core is measured using two methods. The first method consists of a series of toggle switches which are triggered by the dense flowing part of the avalanche. They are placed with intervals of 0.25 m parallel to the pole axis to record the height of the flow up to 7.5 m through contact with the moving snow mass. The sampling frequency is of 1 kHz for the avalanche 7226 and 0.2 kHz for the other avalanches (Figure 3).

[17] The second method uses pressure measurements to determine the position of the highest pressure sensor touched by the avalanche for each time t. In our data we distinguish the dense layer (continuously acting pressure) from the saltation layer (single impacts) by setting a limit of continuous minimum pressure of 20 kPa. All our data with continuous signals show pressures well above this limit, even for very slow avalanches.

[18] The pressure sensors are placed at intervals of 1 m along the pole axis. Figure 4 shows an example of the difference between the two methods. A running average is

Table 1. Summary of the Avalanche Events Measured at the Vallée de la Sionne Test Site During the Winter Seasons 2003–2004 and 2004–2005

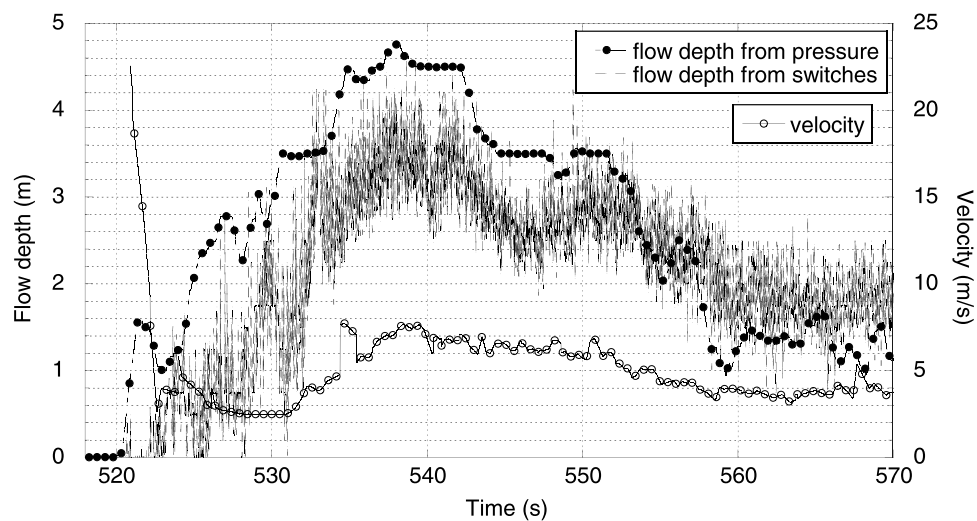| Number	Date	Time, UT	Type
6236	12 Jan 2004	0628	natural, wet-dense
6237	12 Jan 2004	1033	natural, wet-dense
6241	13 Jan 2004	1302	natural, wet-dense
629	19 Jan 2004	1049	artificial, dilute
7226	22 Jan 2005	0310	natural, dry-dense

Figure 4. Flow depth of avalanche 6236 measured with toggle switches (dashed) and derived from pressure measurements (dashed line with circles). The velocity measured 1 m above ground is also shown.

applied to both signals in order to eliminate single discontinuities.

[19] The toggle switches are 0.05 m long and to stay open they require a constant, stationary pressure acting on them; that is, toggle switches detect only the denser part of the avalanche. The more dilute the avalanche, the more discontinuous the signal is. In the case of powder avalanches, the signal is poor. On the contrary, pressure sensors record a continuous signal that, in case of the more dilute avalanches, is strongly fluctuating. The complementary consideration of flow height signals obtained by these two methods allow to determine dense flowing and dilute areas in the avalanche flow structure.

3. Avalanche Observations

[20] We study avalanche data collected during the winter seasons 2003–2004 and 2004–2005 as partially described by *Sovilla et al.* [2004]. We refer to the avalanches by the archive number to enable easy cross reference with further publications. A summary of the avalanches is given in Table 1.

[21] Velocity and pressure measurements at the mast are shown in Figures 5, 6, and 7. The measured forces and velocities have been averaged in time using a running mean over 200 points (0.01 s) and the values between adjacent sensors have been linearly interpolated. The scale of the *y* axis of the two-dimensional plot is always set constant (0–6 m) and the colored area represents the data collected for a specific event. Note that, since pressure measurements are performed above 0.5 m and velocity measurements from 1 to 1.2 m above ground level, the characteristics of the avalanche sliding surface may be lost if the sliding surface is below the lower sensor. The superimposed line represents the maximum dense flow depth measured with toggle switches. The maximum corresponds to the standard deviation $+2\sigma$ from the average depth.

[22] The pressure and velocity plots shown in Figures 5, 6, and 7 show the three main avalanche typologies identified at the site:

[23] 1. Avalanches n. 6236, 6237 and 6241 can be classified as wet-dense. These avalanches released spontaneously because of a combination of new snow overload and air warming. Figure 5 show pressures, velocities and flow depths of avalanche 6236. Before release of avalanche 6236, it has been raining in the lower part of the track. In the upper part of the track, the snow was dry, which allowed avalanche 6236 to develop a small powder layer (identified by optical sensors) which surrounded the wet-dense core. These avalanches were characterized by very low velocities up to about 10 m/s and well defined flow depths. In the powder layer of avalanche 6236 velocities were higher.

[24] 2. Avalanche 7226 is classified as dry-dense. The avalanche released spontaneously probably because of increasing load caused by snowfall. Figure 6 show pressures, velocities and flow depths of this avalanche. The snow was dry along all of the avalanche track. The avalanche developed high velocities and pressures. The flow depth was well defined.

[25] 3. Avalanche 629 is classified as dry-dilute. It was artificially released after a snowfall. The avalanche developed a large powder cloud as shown in Figure 1. It reached high velocities. Because of the large fluctuations and turbulence, velocities were difficult to measure precisely. The avalanche exerted a relatively low pressure on the mast (Figure 7). Because of the poor signals of the flow depth sensors, it was not possible to detect a clear dense core.

[26] Figures 8, 9, and 10 show few seconds of signals from avalanches 6236, 7226 and 629, respectively, corresponding at the zone where maximum pressure is localized.

[27] We characterized the measured avalanche pressures by a combination of at least four basic signals that we have identified as follows:
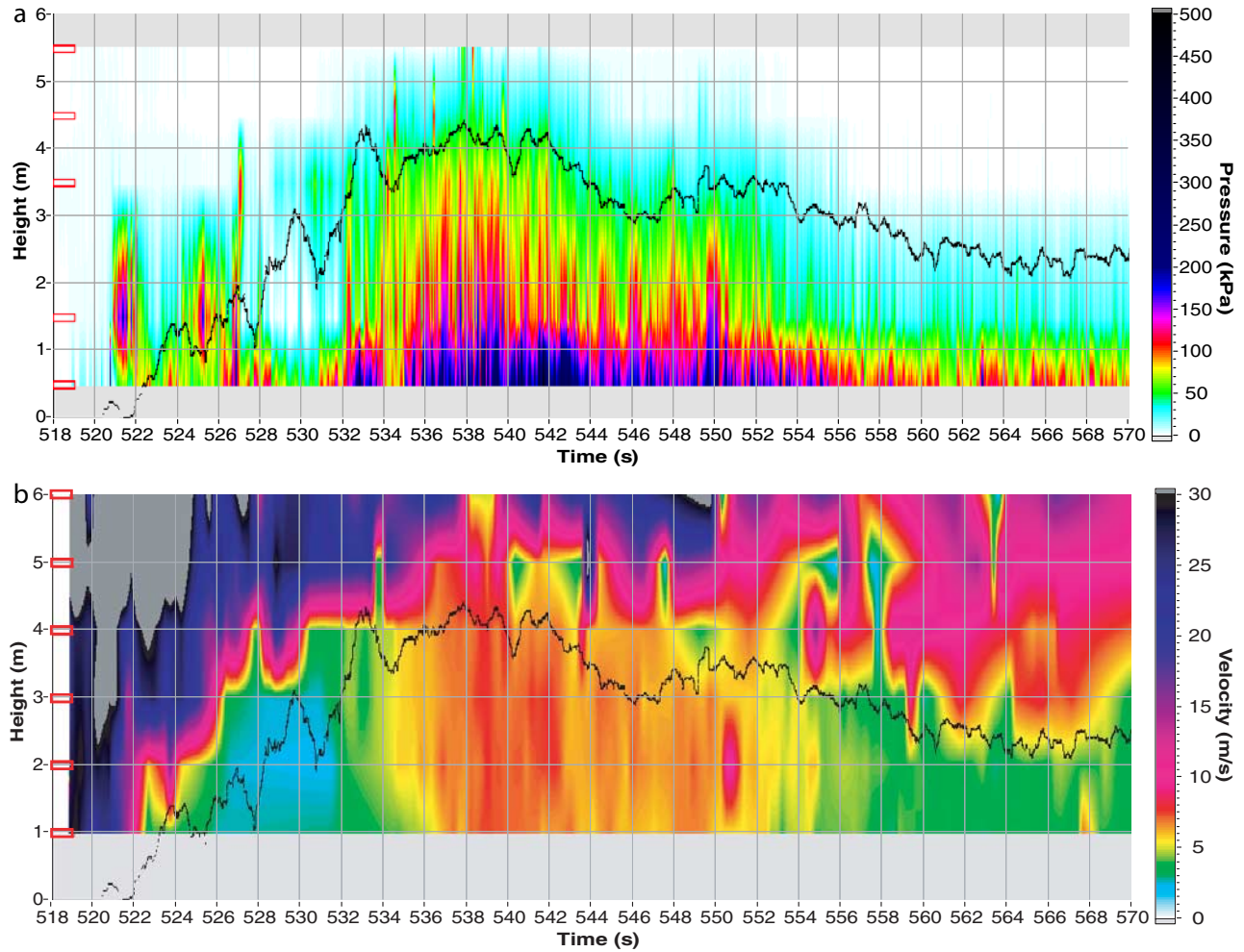
Figure 5. (top) Pressure distribution of avalanche 6236. (bottom) Velocity distribution of avalanche 6236. Rectangles along the *y* axis show the position of the sensors. The superimposed black lines represent the maximum dense flow depth measured with toggle switches.

[28] 1. Signal 1. Stationary pressure with rapid fluctuations. The signal shows a fairly stationary base pressure with rapid fluctuations (Figure 8, avalanche 6236, sensors from 0.5 to 4.5 m). Figure 11 (left) shows a statistical analysis of these signals in the time window 537–539 s. The pressure signal $P(h, t)$ has been normalized with respect to the average pressure $\bar{P}(h)$:

$$\bar{P}(h) = \frac{1}{2} \int_{t_1=537}^{t_2=539} P(h, t) dt. \qquad (1)$$

[29] The signal distribution around the average pressure $\bar{P}$ is shown. Approximatively, the data follows a Gaussian distribution. It is observed that, the larger the depth, the larger the absolute value of pressure (Figure 8) and the corresponding fluctuations are (Figure 11, left). Note that this rule seems not to be respected by the sensor at 1.5 m. This discrepancy is explained by the smaller diameter of this sensor (0.10 m). The other sensors have 0.25 m diameter. This signal is characteristic for wet-dense avalanches and slower parts of dry-dense avalanches.

[30] 2. Signal 2. Stationary pressure with slow fluctuations (Figure 9, avalanche 7226, sensors from 0.5 to 2.5 m).

Figure 11 (right), shows a statistical analysis of these signals in the time window 69–70 s. In contrast to Signal 1, pressure does not increase with depth (Figure 9) and fluctuations are larger close to the surface (Figure 11). Because the signal is not stationary it is impossible to determine if the pressure fluctuations follow Gaussian distribution. This signal is characteristic for the fast moving dense core of dry-dense avalanches.

[31] 3. Signal 3. Short-duration impacts (Figure 9, avalanche 7226, sensors from 3.5 to 5.5 m). There is no stationary pressure, i.e., between each impact, having average duration of few ten milliseconds, the pressure returns to 0. *Schaer and Issler* [2001] identified these peaks as single blocks of snow hitting the sensors. This signal is characteristic of the upper layers of dry-dense avalanches.

[32] 4. Signal 4. Long-duration impacts (Figure 10, avalanche 629, sensors from 1.5 to 5.5 m). Similar to the previous signals but impacts have longer duration on the order of few hundred milliseconds. This signal is characteristic for the avalanche head of the more dilute avalanches.

[33] We can state that all avalanches can be characterized by a succession of these basic signal types. For example, in
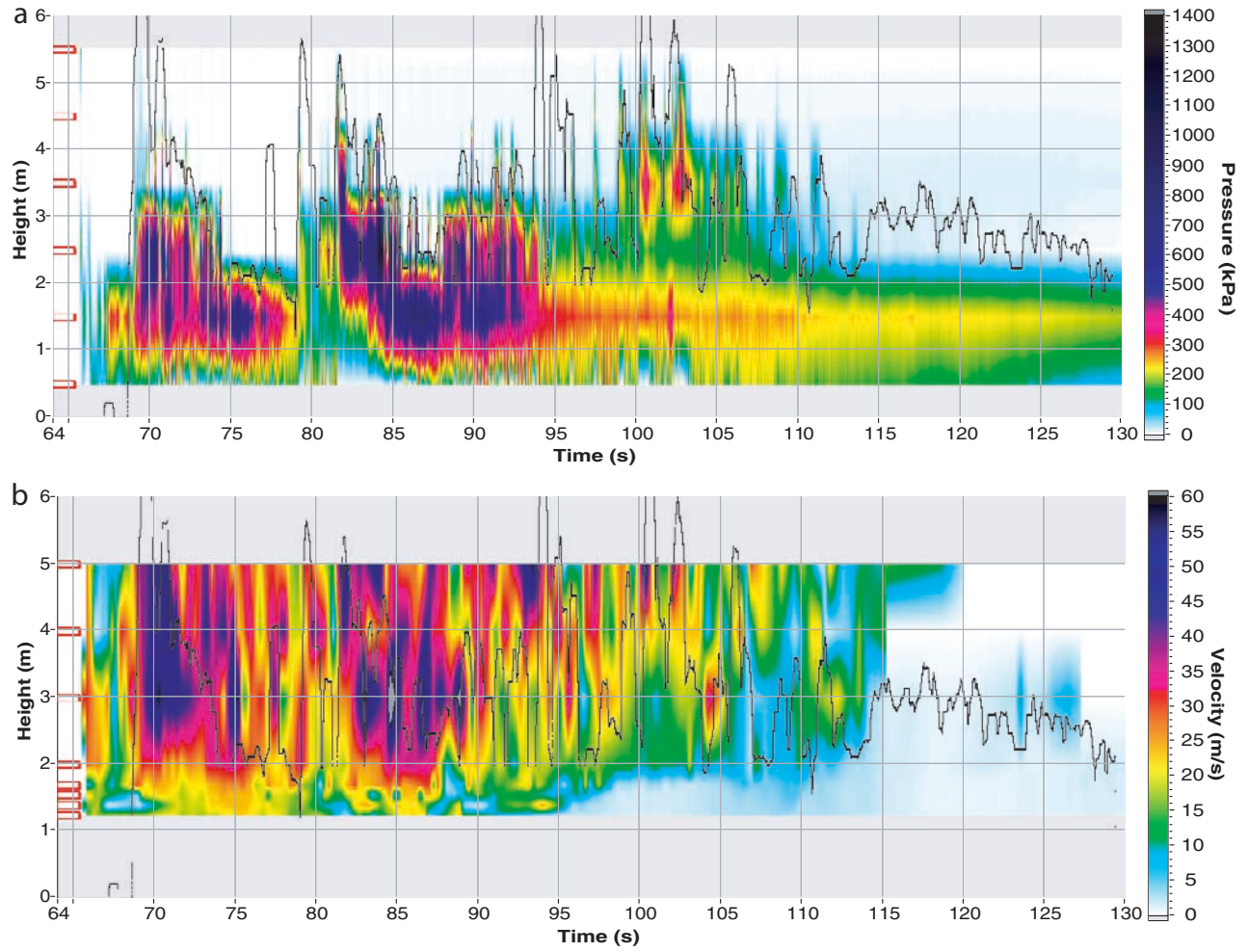
Figure 6. (top) Pressure distribution of avalanche 7226. (bottom) Velocity distribution of avalanche 7226. Rectangles along the *y* axis show the position of the sensors. The superimposed black lines represent the maximum dense flow depth measured with toggle switches.
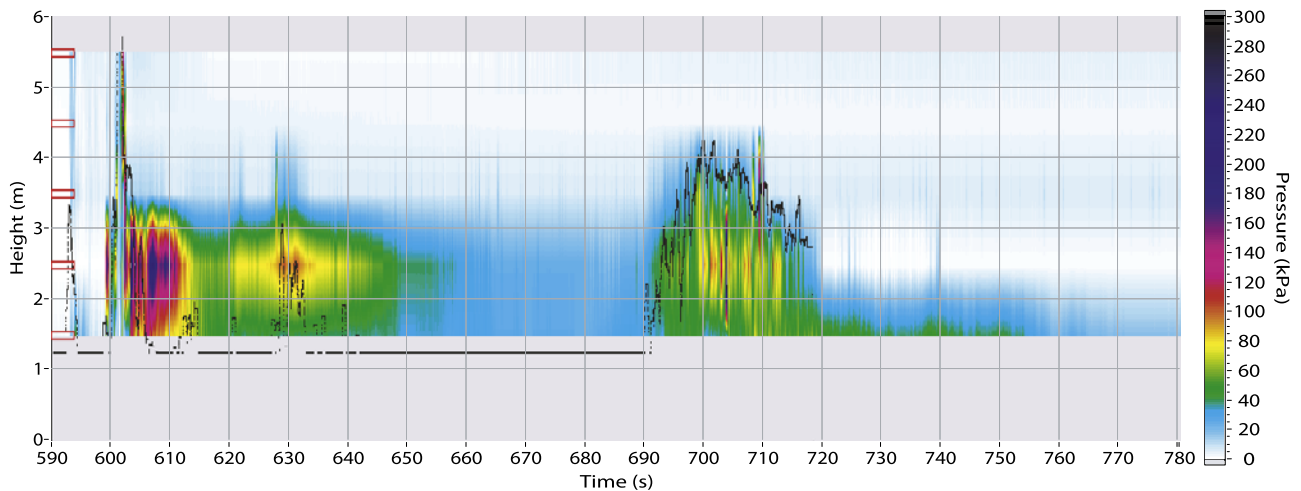
Figure 7. Pressure distribution of avalanche 629. Rectangles along the *y* axis show the position of the pressure sensors.
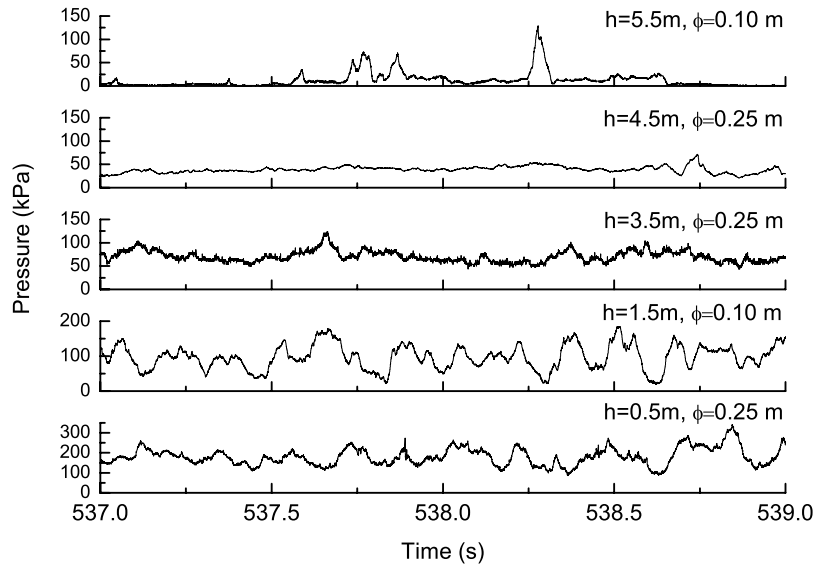
Figure 8. Sample of impact pressure of avalanche 6236. Note the different vertical scaling.

avalanche 7226 (Figure 9) we identify a bottom layer characterized by a signal of type 2. This layer is surmounted by a layer characterized by a signal of type 3.

4. Data Analysis

4.1. Froude Number

[34] To quantitatively characterize the overall flow behavior of avalanches, we calculate the Froude numbers of the avalanches near the mast:

$$Fr = \frac{\langle v_k \rangle}{\sqrt{g \overline{h}_k}}, \tag{2}$$

where $\overline{h}_k$ is the time averaged flow depth at time t_k, $\langle v_k \rangle$ is the depth averaged velocity at the same time and g is the gravitational acceleration.

[35] To analyze the flowing part of the avalanche, we consider the dense layer as a free surface flow and use the flow depth to calculate the Froude number. As a boundary of the denser layer, we use the flow depth $h(t)$ measured with the toggle switches; as a control, the Froude number has been also calculated using the flow depths derived from pressure measurements (bars in Figure 12). Note that for avalanche 629, the depth of a denser flow layer could only be estimated using pressure measurements and it was difficult to identify a distinct dense layer; the Froude number has to be considered a rough estimate.

[36] The average flow depth $\overline{h}_k$ has been calculated for each time t_k using a running average with time window $T = 1$ s:

$$\overline{h}_k = \frac{\cos \alpha}{T} \int_{t_k - \frac{T}{2}}^{t_k + \frac{T}{2}} h(t)\, dt, \tag{3}$$
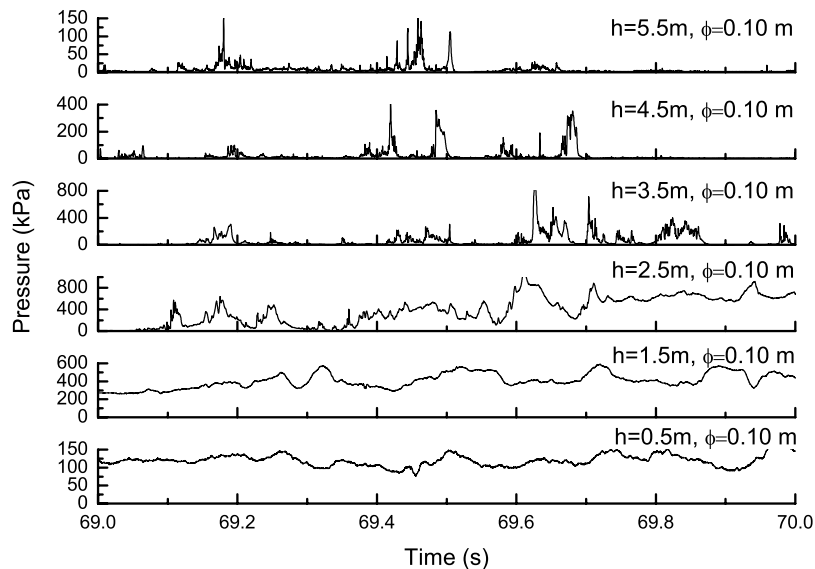

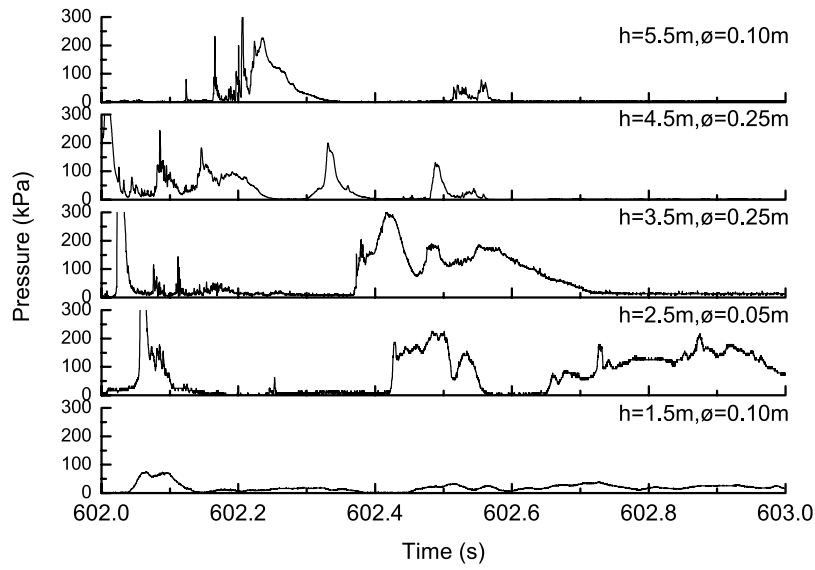**Figure 9.** Sample of impact pressure of avalanche 7226. Note the different vertical scaling.

Figure 10. Sample of impact pressure of avalanche 629.

where $\alpha = 18°$ is the terrain inclination upstream the mast. For each time t_k, the corresponding depth averaged velocity $\langle v_k \rangle$ is

$$\langle v_k \rangle = \frac{\sum_{i=1}^{n} \bar{v}_k(h_i)}{n}, \qquad (4)$$

where n is the number of sensors for which $h_i < \bar{h}_k$, where h_i is the installation height of the sensor and

$$\bar{v}_k(h) = \frac{1}{T} \int_{t_k - \frac{T}{2}}^{t_k + \frac{T}{2}} v(h, t)\, dt. \qquad (5)$$

Thus the depth averaged velocity $\langle v_k \rangle$ refers to measurements only performed inside the dense layer.

[37] In the past, because of the lack of internal velocity data, Froude numbers of avalanches have been calculated referring to frontal velocity and approximative flow depth. On the basis of these evaluations, typical Froude numbers given for dry-dense avalanches were in the order of $5-10$ [*Issler*, 2003; *Schaerer and Salway*, 1980]. Thus dense avalanches have been considered to be supercritical flows [*Schaerer and Salway*, 1980].

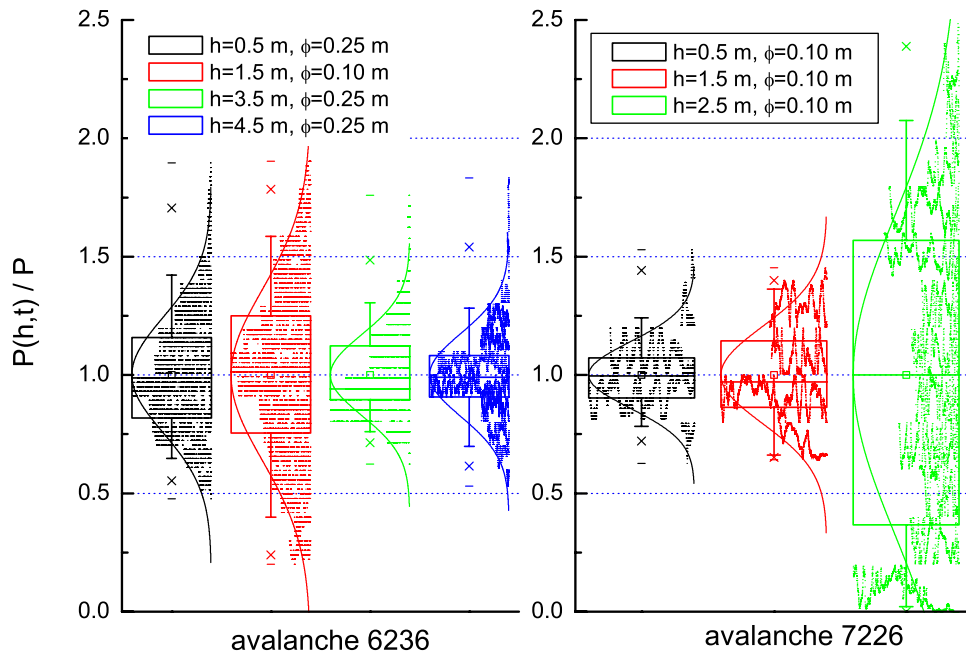[38] New measurements at the Vallée de la Sionne show that the front velocity approximately corresponds to the

Figure 11. Statistical analysis of stationary pressure signals: (left) avalanche 6236 (time window 537–539 s) and (right) avalanche 7226 (time window 69–70 s). The box plots show the mean (square in box), median (line in box), 25/75% quantiles (box), 5/95% quantiles (whiskers), and 0/100% quantiles (cross). Normal distributions have been plotted on the data points.
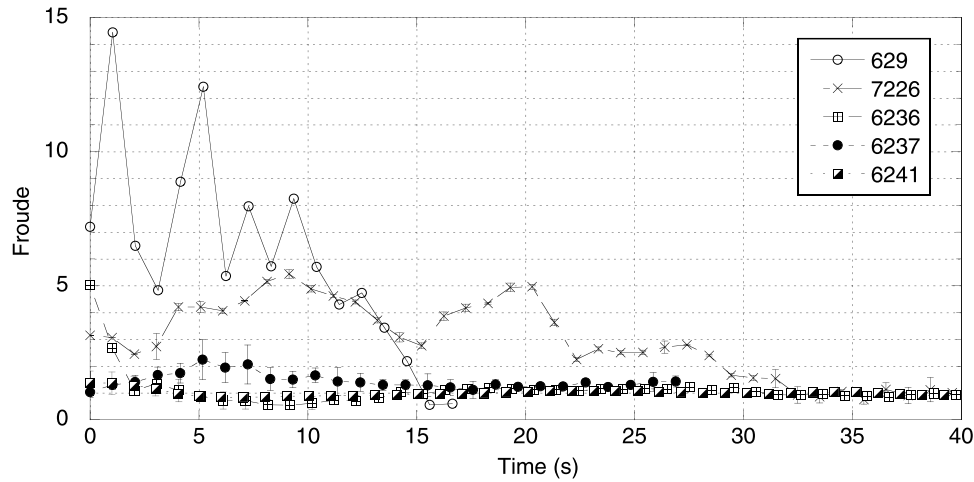
Figure 12. Froude numbers calculated using the flow depth measured with toggle switches. Error bars show the Froude numbers derived from pressure measurements. Time $t = 0$ is the avalanche arrival time at the mast.

average velocity measured in the avalanche saltation layer, while the velocity of the avalanche core is considerably smaller than the front velocity [*Sovilla et al.*, 2008]. Froude numbers calculated with measured dense core velocity and dense core flow height are smaller than previously published (Figure 12). Most avalanches are characterized by Froude numbers lower than 6, including the more destructive ones (avalanche 7226). The only avalanche reaching values of about 15, was the avalanche 629. Recall that for this avalanche, there are no exact data on the vertical extension of its dense part regime. Note that Figure 12 shows only the first 40 s of the avalanches. After 40 s, Froude numbers continue to decrease as shown in Figure 13.

[39] Another important aspect of the Froude number analysis is that wet-dense avalanches but also some parts of the large and destructive dry-dense avalanches move as

subcritical flows ($Fr \leq 1$). Large parts of the faster avalanche (7226) move in a supercritical regime with Froude numbers of about $2-6$. Froude numbers larger then 6 ($Fr > 6-15$) seem to be more associated to dilute avalanches (629).

4.2. Pressure, Velocity, and Drag Coefficient

[40] In avalanche science the pressure exerted by an avalanche on a obstacle is assumed to be proportional to the square of its upstream velocity U and to its density ρ. Shape and rheology effects are taken into account by a drag coefficient C_D [*Salm et al.*, 1990]:

$$P = \frac{1}{2} C_D \rho U^2. \tag{6}$$

[41] Typical values proposed by *Salm et al.* [1990] and used for practical application in Switzerland are a C_D of 2
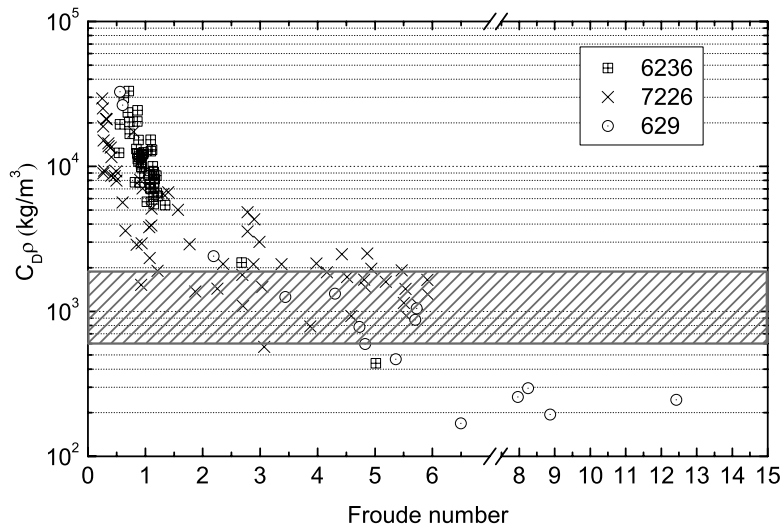

Figure 13. Relationship between Froude number and $C_D\rho$. The gray hatched band indicates the range of $C_D\rho$ values actually used for practical calculations. The upper and lower bounds correspond to $C_D = 6$ and $C_D = 2$, respectively. Note the y axis logarithmic scale.
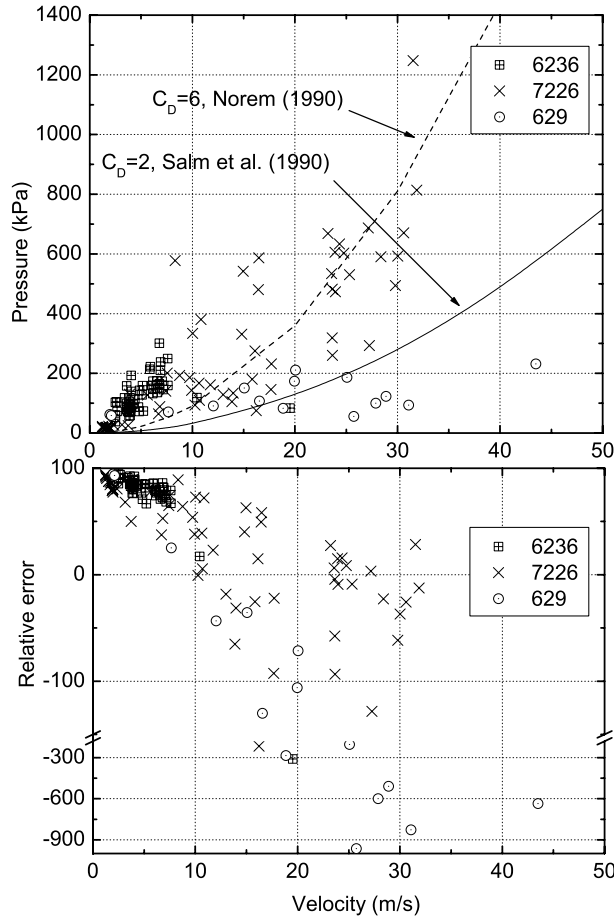
Figure 14. (top) Measured maximum pressure $\bar{P}_{k\max}$ and corresponding average velocity $\bar{v}_k(h)$. The solid line shows the pressure P calculated with equation (6), using $C_D = 2$ as proposed by *Salm et al.* [1990]. The dashed line shows the pressure calculated using $C_D = 6$ found by *Norem* [1990] for wet snow avalanches. We assume a density $\rho = 300$ kg/m^3. (bottom) Relative difference $\frac{P_{k\max} - P}{P_{k\max}}$ between measurements and calculated values for $C_D = 6$.

for small rectangular obstacles and a C_D of 1 for cylindrical ones. *Salm et al.* [1990] proposed to use an average density value of 300 kg/m^3 without any distinction between dry or wet snow. Values of C_D between 2 and 6 have been found for dry, respectively wet snow avalanches at the Norwegian Ryggfonn experimental site by *Norem* [1990].

[42] Figure 14 shows the pressure calculated with equation (6) using a $C_D = 2$ as proposed by *Salm et al.* [1990] for a rectangular obstacle as the mast of Vallée de la Sionne and using $C_D = 6$ as a maximum value found by *Norem* [1990].

[43] On the same plot, pressure data collected at Vallée de la Sionne are plotted. For each avalanche in Table 1, Figure 14 shows maximum pressures plotted against corresponding velocities.

[44] Maximum pressure has been defined as

$$\bar{P}_{k\max} = \max[\bar{P}_k(h_i)] \text{ for } i = 1, .., n, \tag{7}$$

where n is the number of sensors touched by the avalanche and

$$\bar{P}_k(h) = \frac{1}{T} \int_{t_k - \frac{T}{2}}^{t_k + \frac{T}{2}} P(h, t)\, dt. \tag{8}$$

[45] Pressure signals are processed using a moving average with a time window T of 1 s; single particle impacts are not considered. Velocities have been processed using equation (5). We observe that calculated and measured values are not in agreement.

[46] The measured data are used to calculate the factor $C_D\rho$ from equation (8) where $U = \bar{h}_k(h)$ and $P = \bar{P}_{k\max}$. Since we could not measure the density of the flowing avalanches, we assume $\rho = 300$ kg/m^3, as proposed by *Salm et al.* [1990].

[47] Figure 13 shows $C_D\,\rho$ as a function of Froude number. Above $Fr = 2$, $C_D\,\rho$ is approximately independent of the Froude number, while for $Fr < 1$, $C_D\rho$ increases with decreasing Froude number. However, the change between the two behaviors is not at the same position for all avalanches. It lies approximatively at the transition between subcritical and supercritical flow regime, i.e., at $Fr = 1$. We speculate that variation shown in Figure 13 might be due to uncertainties in the determination of the Froude number and in particular in the definition of flow height respectively boundary between dense and saltation layer.

[48] We expect the avalanche density to vary little at low velocities, where the close packing of the particles does not allow much compression. In contrast we expect density to decrease substantially with increasing velocity in the super-critical flow regime. This density variation would result in a Froude dependency of C_D also for higher Froude numbers.

[49] The grey area in Figure 13 shows $C_D\rho$ values between $C_D = 2$ [*Salm et al.*, 1990] and $C_D = 6$ [*Norem*, 1990] for an assumed density $\rho = 300$ kg/m^3.

[50] Especially for slow flow regimes, neglecting the dependency between C_D and Froude number can lead to a serious underestimation of avalanche pressures.

4.3. Avalanche Flow Regimes and Impact Pressure

[51] Combining the signal type classification (Figures 8, 9, and 10) with flow depth, pressure and velocity charts (Figures 5, 6, and 7), we observe that avalanches of Vallée de la Sionne exhibit different characteristics, varying from event to event as well as within the same avalanche. In particular, we observe that under different regimes, the governing physical processes determining the impact pressure seem to change.

4.3.1. Plug Flow Regime

[52] Plug flow regimes were identified in the wet snow avalanche events (6236, 6237, 6241) as well as at the tail of the large dry snow avalanche events (629, 7226). In these cases the mass was moving less than 10 m/s and the Froude numbers were small ($Fr < 2$, and mostly $Fr < 1$, see Figure 12). As depicted in Figure 15 for the wet snow avalanche 6236, the flow plug is characterized by a constant vertical velocity profile with zero shear rate. In this particular case (Figure 15) the at least 4 m thick flow plug is moving at 6 m/s. The avalanche flow height is well defined in the measurement signals and changes slowly with time.
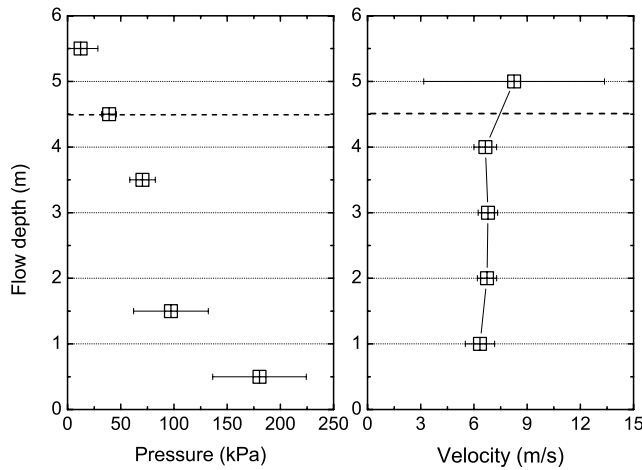
Figure 15. (left) Pressure and (right) velocity profiles of avalanche 6236. Profiles have been obtained by averaging pressure and velocity in the time window 537–539 s, location of the maximum pressures. Bars show the standard deviation (Gaussian distribution). Dashed lines show the approximate local dense flow depth.

Because of the large distance between velocity sensors on the mast (1 m spacing), the exact location of the running surface, and therefore the size of the underlying shear layer, could not be determined. However, we estimate the size of this layer, where frictional and dissipational processes are concentrated, to be less than 0.5 m in height and possibly smaller. The velocity profile measurements of *Dent et al.* [1998] (small dry snow avalanches at the Revolving Door experimental site), the experiments of *Kern et al.* [2004] (dry and wet snow chute experiments) and the earlier experiments of *Nishimura and Maeno* [1989] (small-scale chute experiments with dry snow) all reveal a similar plug flow behavior.

[53] Pressure and velocity signals obtained in the plug flow regime show a steady mean value superimposed with fluctuations. The stationary pressure increases with flow depth in contrast to the velocity profile which remains constant. The largest pressure and fluctuations in pressure are found near the sliding surface. Large fluctuations in velocity exist at the top of the flow, but these are most likely due to variations in flow height as the velocity sensor is alternatively above (no signal) and below the flow surface. Small velocity fluctuations exist near the basal sliding surface as well as in the avalanche core, indicating an enduring, frictional contact between snow granules.

[54] Typically Bingham type constitutive relations [*Dent and Lang*, 1983] are used to explain plug flow regimes since the plug flow height, H, is directly related to the yield stress $\tau_y = \rho g H$. Our data, in comparison to the data of *Dent et al.* [1998], *Nishimura and Maeno* [1989], *Gubler et al.* [1986], and *Kern et al.* [2004], contains the largest plug flow heights measured to date (H > 4 m).

[55] Interestingly, the shear layer would remain concentrated near the basal sliding surface, independent of the size of the overburden in all experiments. A Bingham rheology can thus be conjectured only if the yield stress varies significantly between different snow types and experiments.

However, we did not directly observe this layer and we cannot confirm its existence.

[56] An alternative explanation for the avalanche plug flow regime has been provided by *Bartelt et al.* [2005, 2006] who relate the shear layer height to the injection of fluctuation energy at the base of the avalanche. In their model the flow plug remains because the fluctuation energy supplied at the base is rapidly dissipated by collisional and rubbing contacts between the snow granules in the shear layer and therefore cannot reach the core. For low Froude numbers, the supply of fluctuation energy at the base simply cannot destroy the strong intergranular bonds in the flow plug. The fact that the observed fluctuations in pressure are large near the basal layer does not contradict this hypothesis. Flow plugs have also been observed in granular flows with no cohesion [*GDR MiDi*, 2004].

4.3.2. Impact Pressure in the Plug Flow Regime

[57] *Albert et al.* [1999] measured the drag forces exerted on an object travelling through a granular material in a low-velocity regime (i.e., with grains not fluidized by the motion). His measurements show many analogies to our experimental results of impact pressures in the plug regime. In particular, in Albert's experiments, pressure signals were characterized by a stationary mean value superimposed by fluctuations. Both the mean pressure value and fluctuations increased with the obstacle immersion depth. *Wieghardt* [1975] has obtained similar results with granular experiments.

[58] Albert explained the fluctuating behavior of granular pressure in terms of formation and rupture of force chains within the material and by the stick-slip processes between the grains or grain and obstacle. In contrast to a Newtonian fluid, at low-velocity flow regimes, a stress applied to a granular material propagates inhomogeneously and aniso-tropically through the medium along granular chains, which can be many granular diameters long [*Liu et al.*, 1995]. The stress can increase until it exceeds the cohesion/static friction strength between particles somewhere in the chain. Particles then slip relatively to each other and the stress collapses.

[59] In the case of stress generated by the impact on an obstacle, granular particles are initially stopped by the object and jam around it. At this stage, the drag force at the obstacle increases. The grains start to move (i.e., they are displaced) when the force transmitted by the avalanche bulk to the obstacle exceeds the static friction or the strength of a snow particle somewhere within the force chain. While grains reorganize, the drag force drops. Successive displacements and reorganizations assign a typical stick-slip character to the force; that is, the force oscillates around a stationary value. The oscillations are larger at the bottom of the flow where dilatancy is smaller [*Albert et al.*, 2000] and static friction is larger.

[60] Analyzing pressure signals in the frequency domain, *Albert et al.* [1999] found that the power spectra of the granular signals exhibit a distinct power law typically associated also to other stick-slip processes: $P(f) \sim f^{-2}$. Figure 16 shows the power spectrum of the pressure signals of avalanche 6236. Also the avalanche signal power spectrum exhibit a power law scaling with exponent −2, this bolster our hypothesis that similar stick-slip processes as in granular flows can be seen in our signals.
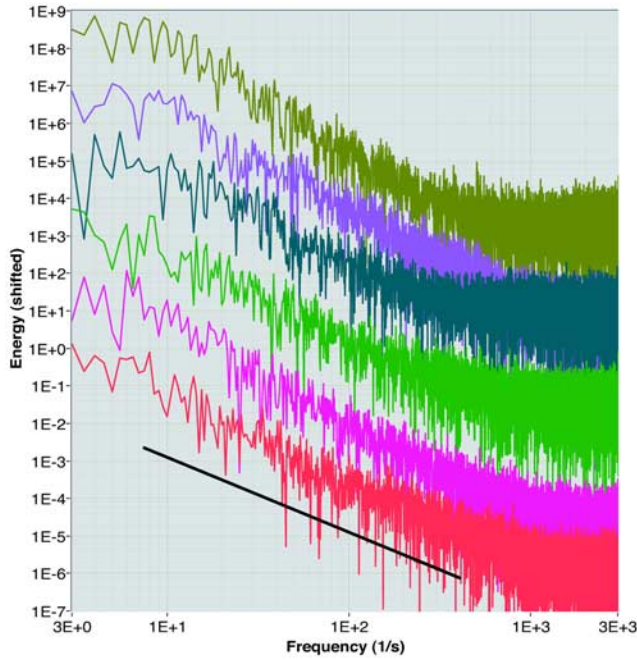
Figure 16. Pressure signal spectrums of avalanche 6236 in the time window 537−539 s for different depths. Signals are shifted vertically for clarity. The reference line has a slope of −2. The lower spectrum corresponds to the pressure signal recorded at 0.5 m; the higher spectrum corresponds to 5.5 m.

[61] The magnitude of the force that the granular flow exerts on the obstacle is a fundamental property of the material and in particular depends on how the internal force chains form and how they are disrupted. Experiments performed at low velocity by *Albert et al.* [1999] show that the average drag force on a cylinder is given by $F = \eta \rho g d_c H^2$, where H is the immersion depth of the cylinder, the dimensionless parameter η characterizes the grain properties, d_c is the cylinder diameter, ρ is the density and g is the gravitational acceleration. In other words, they found no velocity dependence such as in equation (6).

[62] Figure 17 shows that a similar correlation can be found also for snow avalanches. The forces exerted by the avalanches 6236 and 6241 are plotted in function of the mast immersion depth, $\bar{h}_{im}$, which is equal to 0 at the avalanche surface and increases toward the avalanche bottom.

[63] For different immersion depths, we calculated the force acting on the mast using

$$F_{im} = \sum_{i=1}^{n} \frac{\bar{P}(h_i) + \bar{P}(h_{i-1})}{2} A, \qquad (9)$$

where n is the number of sensors for which $h_{im} < h_i < \bar{h}_k$, h_i is the installation height of the sensor, $\bar{h}_k$ is the avalanche depth, $\bar{P}$ is the average pressure and A is the area of the mast to which the pressure refers.

[64] The solid lines are fits of the form $F = \eta \rho g d_c H^{1,5}$. For both avalanches we used $\eta = 17$ and $d_c = 0.6$ corresponding to the mast width. We used a density of 300 and 400 kg/m³ for the avalanches 6336 and 6241, respectively.

[65] These general observations can help to understand the discrepancies shown in Figure 14 between measured pressure and pressure calculated with equation (8) which increase at low velocity. At low velocity the drag on a vertical rod is mainly given by a static component of the form $F = \eta \rho g d_c^m H^n$. This is in good agreement with granular experiments by *Albert et al.* [1999] and *Wieghardt* [1975], except for the different coefficients η, m, n. Presumably, these differences are attributable to different material properties which include viscosity, compressibility, and cohesion effects.

4.3.3. Shear Flow Regimes

[66] A fundamentally different flow regime was identified in the dry snow avalanches 629 and 7226. We observed a sheared velocity profile when the avalanche was moving at velocities between 10 and 30 m/s (Fr approximately 6). Figure 18 depicts the pressure and velocity profiles of avalanche 7226. In this case the sheared layer is located between 1 and 3 m and the average shear rate is $\dot{\gamma} = 17 \ s^{-1}$. The velocity profile was constructed by averaging the measured velocities over a two second time period when the applied pressure was maximum (between 69 s and 71 s). We found that the measured shear rate can change abruptly because of sudden changes in flow velocity (see Figure 6, bottom, which depicts the local velocity of avalanche 7226 at the mast). For avalanche 7226 the height sensors revealed flow waves with changes of amplitudes of 2 m with periods of a few seconds.

[67] We again divided the measured pressure and velocity signals into time-averaged mean values superimposed with a fluctuating part. In contrast to the plug flow regime the mean pressure and amplitude of fluctuations do not increase with depth. The largest pressures are located in the avalanche core between 1.5 m and 3 m. The largest fluctuations are located near the free surface of the flow; however, these oscillations might be produced by flow height and density variations.

[68] To distinguish between frictional and collisional flow regimes, *Savage and Hutter* [1989] proposed the dimensionless number

$$R_s = \frac{\rho \dot{\gamma}^2 d^2}{\rho g z}, \qquad (10)$$

where d is the grain diameter and z is the depth below the avalanche surface. For $R_s < 0.1$ (as a crude estimate) they proposed that the avalanche is in a flow regime where enduring particle contacts in which intergranular rubbing and sliding are the dominant frictional mechanism. For the layer situated close to the sliding surface, the condition for the flow to be in the frictional regime is satisfied by particles having diameters smaller than 0.1 m, which is certainly the case. Particle size profiles made in avalanche debris seldom contain particle sizes larger than 0.1 m at this depth some 3 m below the surface. Observations of near surface particle size distributions (B. McArdell, personal communication, 2006) show that the most frequent particle size is approximately 0.1−0.2 m. Larger particles can exist at the top surface because of inverse segregation [*Kern*, 2000], indicating the possibility of a frictional or collisional flow regime depending on particle size.
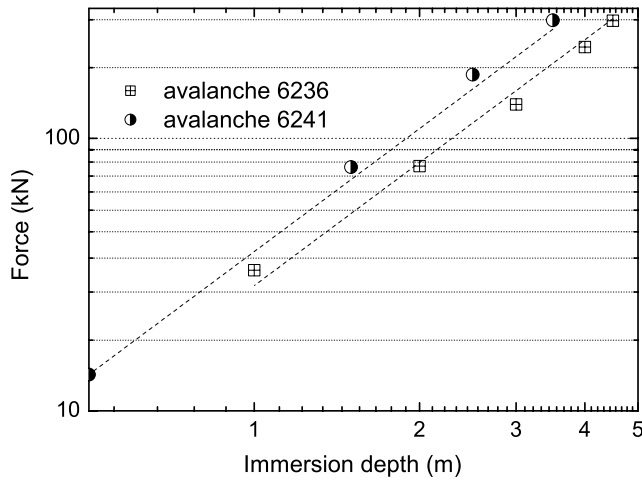
Figure 17. Depth dependence of the drag force measured at the mast. The dashed lines are fits of the form $F = \eta \rho g d_c H^{1,5}$.

[69] However, this ad hoc and strict distinction between collisional and frictional shear flow regimes should be applied with caution. It is more likely that both frictional and collisional processes exist simultaneously, especially since snow avalanches contain a particle size distribution and cannot be characterized by a single grain size d. This view is shared by *Louge and Keast* [2001] who describe granular flows on flat, frictional inclines by considering both enduring frictional contacts and collisions with much shorter impulsive interactions. Our measurements reveal that the shear regime is associated with considerable granular agitation and therefore particle fluctuations and less dense, diluter flows. It appears that the flux of fluctuation energy in an avalanche increases with flow velocity and is less likely to be dissipated by intergranular collisions/rubbing in a dry avalanche than in a wet snow avalanche [*Bartelt et al.*, 2005, 2006].

4.3.4. Impact Pressures in the Shear Regime

[70] The mean pressure measured in the shear flow regime can be very high up to 800 kPa for avalanche 7226 (Figure 9). Figure 14, top plot, shows measured pressure and calculated pressure using equation (8) with $C_D = 2$ as proposed by the Swiss procedure, and $C_D = 6$ as found by *Norem* [1990] for wet snow avalanches. For both calculations we assume a density of 300 kg/m^3.

[71] The plot shows a big scattering in the data. In order to better understand the differences, we calculated the relative divergence between calculations with $C_D = 6$ and measurement (Figure 14, bottom plot). The general agreement between measured and calculated pressure is very poor. For velocities below 20 m/s, with an increasing probability of a plug flow regime, the difference from the calculated values increases progressively, suggesting a contribution from a static pressure (velocity-independent) component as already stated for the plug flow regime.

[72] For velocities above 30 m/s, moving toward a highly agitated regime (avalanche 629), the measured pressures are lower than the calculated pressure. We believe that the higher flow velocities are associated with less dense flows and that the discrepancy between the measured and calcu-

lated pressures is due to the fact that we employed a too high density (300 kg/m^3) in our calculations.

4.4. Conclusion and Outlook

[73] The two primary results that we have obtained from the Vallée de la Sionne pressure and velocity measurements are:

[74] 1. Both plug and shear flow regimes can exist in dense snow avalanches. The plug flow velocity profiles were found in subcritical ($Fr < 1$) wet and dry snow avalanches; the shear flow regimes where found in supercritical ($Fr > 1$), dry snow avalanches. A single avalanche can contain both regimes.

[75] 2. The measured impact pressure in the subcritical plug flow regime did not show a velocity dependence, whereas the supercritical shear flows had a definite velocity dependence.

[76] Thus the real-scale experiments at the Vallée de la Sionne reveal that as an avalanche decelerates and the flow changes from a rapid, dilute shear flow to a slow, plug-like movement, obstacle drag becomes increasingly velocity-independent. The parameters governing the transition are not well understood; however, the boundaries between the different regimes may be empirically described for now by a Froude number dependency. Interestingly, measured basal shear stresses in snow avalanches are also not velocity-dependent at low velocities [*Platzer et al.*, 2007]. At low velocities, it appears that the production of random kinetic energy at the basal shear layer decreases, allowing interparticle forces to dominate the frictional behavior. Nondeforming flow plugs can then form in the core of the avalanche. This is similar to the macroviscous behavior of granular systems. In fact, our results are similar to data obtained from experiments with granular material by a series of investigators [*Albert et al.*, 1999; *Wassgren et al.*, 2003]. The measured pressure signals are subsequently dominated by
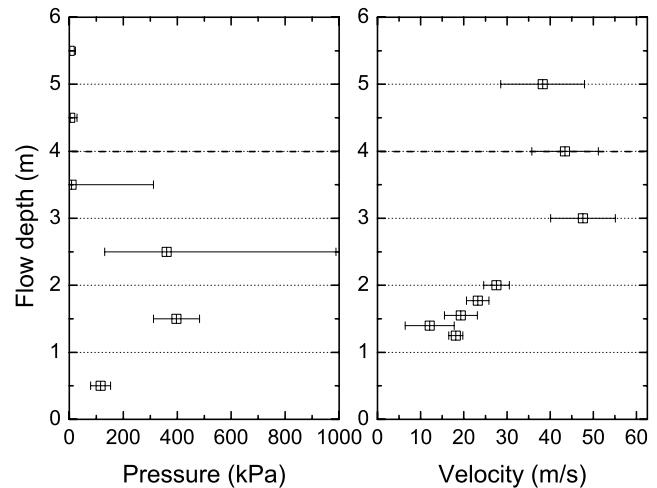

Figure 18. (left) Pressure and (right) velocity profiles of avalanche 7226. Profiles have been obtained by averaging pressure and velocity in the time window 69–71 s, location of the maximum pressures. Bars show the standard deviation (Gaussian distribution for the sensors up to 1.5 m and logarithmic distribution for the higher sensors). Dashed lines show the approximate local dense flow depth.

noninertial (velocity-independent) effects. Future work must concentrate on quantifying nonlinear processes driving the flow regime transition.

[77] Most importantly, the results of these initial investigations will have direct consequences for the practical design of defense structures in the runout zone of real avalanches. Recall, for example, that buildings can be placed in the runout zone of avalanches in Switzerland (and elsewhere) only when the avalanche velocity is less than 10m/s that is, when the avalanche is probably in a subcritical (velocity-independent pressure) flow regime.

[78] One problem that we could not resolve in this paper is the proper downscaling of avalanches. The similarity of our data to granular material imply that, under controlled conditions, experiments performed with granular material may be used to reproduce the characteristics of snow avalanches. The Froude numbers found in Vallée de la Sionne suggest that $Fr > 6$ should not be used when attempting to physically model dense snow avalanches. However, the similarity of Froude number dependency on obstacle drag forces, observed in both small-scale granular avalanches and large snow avalanches, is no proof that the similarity is due to the same underlying effects. Froude scaling ignores frictional processes at the base of the flow which, for real-scale avalanches, are not understood at the macrocontinuum or micromechanical level.

References

Albert, I., P. Tegzes, B. Kahng, R. Albert, J. G. Sample, M. Pfeifer, A.-L. Barabási, T. Vicsek, and P. Schiffer (2000), Jamming and fluctuations in granular drag, *Phys. Rev. Lett.*, 84(22), 5122–5125.

Albert, R., M. A. Pfeifer, A.-L. Barabási, and P. Schiffer (1999), Slow drag in granular medium, *Phys. Rev. Lett.*, 82(1), 205–208.

Ammann, W. J. (1999), A new Swiss test site for avalanche experiments in the Vallée de la Sionne/Valais, *Cold Reg. Sci. Technol.*, 30, 3–11.

Bartelt, P., O. Buser, and M. Kern (2005), Dissipated work, stability and the internal flow structure of granular avalanches, *J. Glaciol.*, 51(172), 1–14.

Bartelt, P., O. Buser, and K. Platzer (2006), Fluctuation-dissipation relations for granular snow avalanches, *J. Glaciol.*, 52(179), 631–643.

Dent, J. D., and T. E. Lang (1983), A biviscous modified Bingham model of snow avalanche motion, *Ann. Glaciol.*, 4, 42–46.

Dent, J. D., K. J. Burrell, D. S. Schmidt, M. Y. Louge, E. Adams, and T. G. Jazbutis (1998), Density, velocity and friction measurements in a dry snow avalanche, *Ann. Glaciol.*, 26, 247–252.

GDR MiDi (2004), On dense granular flows, *Eur. Phys. J. E.*, 14, 341–365.

Gubler, H., M. Hiller, G. Klausegger, and U. Suter (1986), Messungen an Fliesslawinen. Zwischenbericht 1986, *Mitt. 41*, Eidg. Inst. fuer Schnee-und Lawinenforsch., Weissfluhjoch, Switzerland.

Issler, D. (1999), European avalanche test sites. Overview and analysis in view of coordinated experiments, *Mitt. 59*, Eidg. Inst. fuer Schnee- und Lawinenforsch., Davos, Switzerland.

Issler, D. (2003), Experimental information on the dynamics of dry-snow avalanches, in *Dynamic Response of Granular and Porous Materials Under Large and Catastrophic Deformations, Lecture Notes Appl. Comput. Mech.*, vol. 11, edited by K. Hutter and N. Kirchner, pp. 109–160, Springer, Berlin.

Kern, M. (2000), Inverse grading in granular flow, Ph.D. thesis, Ecole Polytech. Fed. de Lausanne, Lausanne, Switzerland.

Kern, M. A., F. Tiefenbacher, and J. N. McElwaine (2004), The rheology of snow in large chute flows, *Cold Reg. Sci. Technol.*, 39, 181–192.

Liu, C.-H., S. R. Nagel, D. A. Schecter, S. N. Coppersmith, S. Majumdar, O. Narayan, and T. A. Witten (1995), Force fluctuations in bead packs, *Science*, 269, 513–515.

Louge, M. Y., and S. Keast (2001), On dense granular flows down flat frictional inclines, *Phys. Fluids*, 5(13), 1213–1233.

Louge, M. Y., R. Steiner, S. Keast, R. Decker, J. Dent, and M. Schneebeli (1997), Application of capacitance instrumentation to the measurement of density and velocity of flowing snow, *Cold Reg. Sci. Technol.*, 25, 47–63.

McClung, D. M., and P. A. Schaerer (1985), Characteristics of flowing snow and avalanche impact pressures, *Ann. Glaciol.*, 6, 9–14.

McElwaine, J. N., and B. Turnbull (2005), Air pressure data from the Vallée de la Sionne avalanches of 2004, *J. Geophys. Res.*, 110, F03010, doi:10.1029/2004JF000237.

Nishimura, K., and N. Maeno (1989), Contribution of viscous forces to avalanche dynamics, *Ann. Glaciol.*, 13, 202–206.

Norem, H. (1990), Ryggfonn prosjektet; Forslag til beregning av dimensionerende snoskredlast mot mastekonstruktioner, *Tech. Rep. 581200-16*, Norw. Geotech. Inst., Oslo.

Norem, H., T. Kvisterøy, and B. D. Evensen (1985), Measurement of avalanche speeds and forces: Instrumentation and preliminary results of the Ryggfonn project, *Ann. Glaciol.*, 6, 19–22.

Norem, H., F. Irgens, and B. Schieldrop (1987), A continuum model for calculating snow avalanche velocities, in *Avalanche Formation, Movement and Effects: Proceedings of the Davos Symposium, September 1986*, edited by B. Salm and H. Gubler, *IAHS Publ.*, 162, 363–378.

Norem, H., F. Irgens, and B. Schieldrop (1989), Simulation of snow-avalanche flow in run-out zones, *Ann. Glaciol.*, 13, 218–225.

Platzer, K., P. Bartelt, and M. Kern (2007), Measurements of dense snow avalanche basal shear to normal stress ratios (S/N), *Geophys. Res. Lett.*, 34, L07501, doi:10.1029/2006GL028670.

Salm, B., A. Burkard, and H. U. Gubler (1990), Berechnung von Fliesslawinen: Eine Anleitung fuer Praktiker mit Beispielen, *Mitt. 47*, Eidg. Inst. Schnee- und Lawinenforsch., Davos, Switzerland.

Savage, S. B., and K. Hutter (1989), The motion of a finite mass of granular material down a rough incline, *J. Fluid Mech.*, 199, 177–215.

Savage, S. B., and K. Hutter (1991), The dynamics of avalanches of granular materials from initiation to run-out. part I. Analysis, *Acta Mech.*, 86(1–4), 201–223.

Schaer, M., and D. Issler (2001), Particle densities, velocities and size distribution in large avalanches from impact-sensor measurements, *Ann. Glaciol.*, 32, 321–327.

Schaerer, P. A., and A. A. Salway (1980), Seismic and impact-pressure monitoring of flowing avalanches, *J. Glaciol.*, 26(94), 179–187.

Sovilla, B., and P. Bartelt (2002), Observations and modelling of snow avalanche entrainment, *Nat. Hazards Earth Syst. Sci.*, 2, 169–179.

Sovilla, B., et al. (2004), Avalanche dynamics experimental site Vallée de la Sionne, Arbaz, Vallais, *Rep. 753*, Eidg. Inst. fuer Schnee- und Lawinenforsch., Davos, Switzerland.

Sovilla, B., P. Burlando, and P. Bartelt (2006), Field experiments and numerical modeling of mass entrainment in snow avalanches, *J. Geophys. Res.*, 111, F03007, doi:10.1029/2005JF000391.

Sovilla, B., M. Schaer, and L. Rammer (2008), Measurements and analysis of full-scale avalanche impact pressure at the Vallée de la Sionne test site, *Cold Reg. Sci. Technol.*, 51(2–3), 122–137, doi:10.1016/j.coldregions.2007.05.006.

Tiefenbacher, F. (2003), *Vom konstitutiven Verhalten fliessenden Schnees*, Ph.D. thesis, Univ. Basel, Basel, Switzerland.

Tiefenbacher, F., and M. A. Kern (2004), Experimental devices to determine snow avalanche basal friction and velocity profiles, *Cold Reg. Sci. Technol.*, 38, 17–30.

Vallet, J., U. Gruber, and F. Dufour (2001), Photogrammetric avalanche volume measurements at Vallée de la Sionne, Switzerland, *Ann. Glaciol.*, 32, 141–146.

Vallet, J., B. Turnbull, S. Joly, and F. Dufour (2004), Observations on powder snow avalanches using videogrammetry, *Cold Reg. Sci. Technol.*, 39, 153–159.

Wassgren, C. R., J. A. Cordova, R. Zenit, and A. Karion (2003), Dilute granular flow around an immersed cylinder, *Phys. Fluids*, 15(11), 3318–3330.

Wieghardt, K. (1975), Experiments in granular flow, *Annu. Rev. Fluid Mech.*, 7, 89–114.

———————
P. Bartelt, M. Kern, M. Schaer, and B. Sovilla, Swiss Federal Institute for Snow and Avalanche Research, Flüelastrasse, 11, CH-7260 Davos, Switzerland. (sovilla@slf.ch)